



RESEARCH LETTER

10.1002/2015GL063986

Key Points:

- High reservoir temperatures enhance fine particle mobilization and migration
- Fine particle migration has greater effect on geothermal reservoirs than on conventional fields
- The analytical model is consistent with geothermal production history

Supporting Information:

- Text S1 and Figure S1

Correspondence to:

Z. You,
zyou@asp.adelaide.edu.au

Citation:

You, Z., P. Bedrikovetsky, A. Badalyan, and M. Hand (2015), Particle mobilization in porous media: Temperature effects on competing electrostatic and drag forces, *Geophys. Res. Lett.*, *42*, 2852–2860, doi:10.1002/2015GL063986.

Received 26 MAR 2015

Accepted 27 MAR 2015

Accepted article online 1 APR 2015

Published online 28 APR 2015

Particle mobilization in porous media: Temperature effects on competing electrostatic and drag forces

Zhenjiang You¹, Pavel Bedrikovetsky¹, Alexander Badalyan¹, and Martin Hand²

¹Australian School of Petroleum, University of Adelaide, Adelaide, South Australia, Australia, ²South Australian Centre for Geothermal Energy Research, Institute of Mineral and Energy Resources, University of Adelaide, Adelaide, South Australia, Australia

Abstract The fluid flow in natural reservoirs mobilizes fine particles. Subsequent migration and straining of the mobilized particles in rocks greatly reduce reservoir permeability and well productivity. This chain of events typically occurs over the temperature ranges of 20–40°C for aquifers and 120–300°C for geothermal reservoirs. However, the present study might be the first to present a quantitative analysis of temperature effects on the forces exerted on particles and of the resultant fines migration. Based on torque balance between electrostatic and drag forces acting on attached fine particles, we derived a model for the maximum retention concentration and used it to characterize the detachment of multisized particles from rock surfaces. Results showed that electrostatic force is far more affected than water viscosity by temperature variation. An analytical model for flow toward wellbore that is subject to fines migration was derived. The experiment-based predictive modeling of the well impedance for a field case showed high agreement with field historical data (coefficient of determination $R^2 = 0.99$). It was found that the geothermal reservoirs are more susceptible to fine particle migration than are conventional oilfields and aquifers.

1. Introduction

Fine particle mobilization, migration, and straining in narrow pore throats, with consequent permeability decline, occur in a broad range of environmental, geophysical, and engineering problems or processes [Gaillard *et al.*, 2007; Chen *et al.*, 2008]. Particle transport and retention significantly affects groundwater flow [Saiers and Ryan, 2005], water injection and production in artesian and geothermal wells [Rosenbrand *et al.*, 2014, 2015], propagation of contaminants, viruses, and bacteria in aquifers [Ederly *et al.*, 2011; Bradford *et al.*, 2012, 2014], degradation of streambed habitat by siltation [Rehg *et al.*, 2005], production of oil and gas [Bedrikovetsky, 1993], geosequestration of carbon dioxide [Mangane *et al.*, 2013], and underground disposal of industrial and radioactive wastes [Bradford *et al.*, 2012, 2013]. The stress alteration resulting from fine particle straining explains hydrologic responses to earthquakes and can even trigger earthquakes [Liu and Manga, 2009; Manga *et al.*, 2012]. Thus, an accurate laboratory-based mathematical model of fine particle migration in porous and fractured media is essential for reliable prediction of oil and water production, design of enhanced geothermal systems, protecting groundwater against contamination, assessing the safety of long-term hazardous waste sites, and determining remediation strategies for contaminated sites [Bartels *et al.*, 2002; Nemati *et al.*, 2003; Boutt *et al.*, 2006; You *et al.*, 2014].

Permeability decline induced by particle retention in porous media is explained by detachment and mobilization of reservoir fine particles and their migration and straining in narrow pore throats. Particle detachment leads to insignificant increase of reservoir permeability, whereas cutting off a flow path by particle straining in narrow pore throats significantly reduces permeability. Therefore, mathematical models of permeability that consider particle straining usually disregard the effect of particle detachment [Bedrikovetsky, 1993; Khilar and Fogler, 1998]. A particle on the pore surface is subject to electrostatic, drag, lifting, and gravitational forces, as shown in Figure 1. Particle mobilization occurs where the torque of detaching hydrodynamic drag and lifting forces exceeds that of attaching electrostatic and gravitational forces; i.e., the torque balance is the condition of mechanical equilibrium for particles [Freitas and Sharma, 2001; Bradford *et al.*, 2013]. Although salinity, pH, and velocity effects on the forces exerted on particles have been comprehensively investigated [Khilar and Fogler, 1998; Israelachvili, 2011], the quantitative analysis of temperature effects on these forces and the consequent fines migration had been absent. Since high temperature is common in geothermal field applications, the current work involves the laboratory-

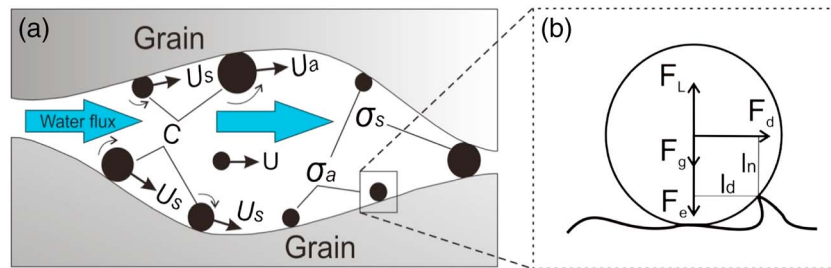


Figure 1. Particle straining, attachment, and detachment in porous media: (a) cross section of a pore throat and (b) illustrating forces acting on the attached fine particles (c , σ_a , and σ_s are suspended, attached, and strained concentrations, respectively; U and U_s are velocities of fluid and particles, respectively; F_d , F_e , F_g , and F_L are drag, electrostatic, gravitational, and lifting forces, respectively; l_d and l_n are lever arms for drag and electrostatic forces, respectively).

based prediction of fines migration under the field conditions of high temperature. Here we develop a model that is readily applicable for field conditions.

The traditional kinetics model for colloidal-suspension transport assumes nonequilibrium particle release, which is proportional to the difference between the current and equilibrium values of variables such as velocity, ionic strength, pH, and temperature [Elimelech *et al.*, 1998]. However, the kinetics model fails to reflect the instant permeability response to variation in these variables, which has been observed in many laboratory tests [Ochi and Vernoux, 1998]. The traditional model also fails to capture the microscale condition of mechanical equilibrium for particles. However, the maximum retention concentration, as a function of velocity, ionic strength, and temperature, can be derived from the particle torque balance condition and is capable of modeling the instant particle release [Bedrikovetsky *et al.*, 2011, 2012]. Thus, this method is free of the above mentioned shortcomings and is used in the present study. The maximum retention function derived in Bedrikovetsky *et al.* [2011, 2012] for multilayers of monosized particles exhibits a convex form with respect to velocity. In the current work, we develop a new model for detachment of monolayer size-distributed particles, which results in different forms of the maximum retention function versus velocity.

Laboratory flow-through tests on natural reservoir cores with varying piecewise constant flow velocities and water salinities show that the core permeability stabilizes significantly later than the moment corresponding to when one pore volume has been injected [Ochi and Vernoux, 1998; Oliveira *et al.*, 2014]. This delayed-stabilization effect is attributed to the slow particle drift near pore walls and to particle sliding or rolling along rock surfaces. Particle transport in the boundary layers, and in the bulk of carrier fluid, is reflected by a two-velocity model [Yuan and Shapiro, 2011; Bradford *et al.*, 2012, 2014; Sefrioui *et al.*, 2013]. The model developed in the current work applies specifically to the case where a rapid mass exchange occurs between fast and slow particle populations across each pore. The capture-free run of particles can span numerous pore lengths. Therefore, the mass exchange is assumed to be significantly faster than particle capture by rocks. It results in equal concentrations of particles in the fast and slow fluxes, yielding a single-velocity model.

In the present work, the detailed study of temperature dependence of electrostatic constants found that the electrostatic force is far more affected than water viscosity by temperature variation. The former effect results in significantly higher decline of permeability and well productivity due to fines migration at high temperatures. Also, analytical models for flow through natural cores and flow toward wellbores under fines migration were derived. The laboratory-based analytical models were tested against historical data of Salamander geothermal well exploitation (Otway Basin, Australia), accounting for the temperature dependency of the maximum retention concentration. The well impedance growth predicted by the model agreed with that from field historical data, with the coefficient of determination $R^2 = 0.99$. The model predicted that the likelihood of fines migration would be greater in geothermal wells than in conventional oil and artesian wells.

2. Physics of Particle Mobilization and Straining in Porous Media

Fine particle mobilization is determined by the exerting forces depicted in Figure 1b. Formulas for drag (F_d) and lifting (F_L) forces can be found in Altmann and Ripperger [1997] and Bradford *et al.* [2013]. The ratio F_L/F_d

does not exceed 0.0004, for velocity U varying from 10^{-5} to 10^{-3} m/s, particle radii r_s , from 1 to 5 μm , ionic strength γ from 0.025 to 0.20 M NaCl, and temperature T from 25°C to 130°C, which are the conditions we covered in this study. Therefore, the lifting force F_L can be disregarded. Under these conditions, the gravitational force F_g can also be disregarded, since the ratio F_g/F_d is below 0.02. Figure 1 does not show the Brownian diffusive force due to collisions, which is modeled as Gaussian noise [see Kim and Zydney, 2004]. Within the above parameter ranges, the ratio between the Brownian and drag forces does not exceed 0.05, allowing the Brownian force to be disregarded. Finally, the torque balance condition for characterization of the particle release from rock surfaces is expressed as

$$F_d(U, r_s)l(r_s) = F_e(\gamma, r_s), \quad l = l_d/l_n \quad (1)$$

where F_e is the electrostatic force acting on the particle and l_d and l_n are lever arms for drag and electrostatic forces, respectively. The lever arm ratio l is determined by either asperities of the rock surface or contact deformation of particles on the rock [Freitas and Sharma, 2001; Bradford et al., 2013]. Formulas for electrostatic force and potentials are given in the supporting information. The transcendental equation (1) for the particle size r_s determines the critical radius of particles which satisfies torque balance condition at certain velocity U and ionic strength γ . Any particles larger than this size are detached from rock surfaces. The critical particle radius r_{scr} can be expressed as

$$r_{scr} = r_s(U, \gamma) \quad (2)$$

Function r_s monotonically decreases with U and increases with γ . It indicates that the size of particles dislodged from the rock surface by drag force decreases with increasing U or decreasing γ . The sequence of particle detachments in response to variation in U and γ with equation (2) leads to the following form of the maximum retention function σ_{cr} :

$$\sigma_{cr}(U, \gamma) = \int_0^{r_{scr}(U, \gamma)} \Sigma_a(r_s) dr_s \quad (3)$$

Differentiation of equation (3) with respect to r_s results in the size distribution of attached particles $\Sigma_a(r_s)$, leading to a method for laboratory determination of attached particle size distribution in rocks.

The lever arm ratio l in equation (1) is calculated from Hertz contact theory of particle and rock deformation [Bradford et al., 2013; Kalantariasl and Bedrikovetsky, 2014]; for sandstone rocks and illite/chlorite fine particles, $l = 0.0021$. Typical forms of the maximum retention function versus U and γ as calculated from equations (2) and (3) are shown in Figure 2. Point I in the figure corresponds to the initial concentration of attached particles σ_{ai} . A velocity increase from zero to U_B (ionic strength decrease from γ_1 to γ_2) does not lift particles. The first fine particle appears at point B in the figure. Further velocity increase to U_C (ionic strength decrease to γ_3) causes the release of particles by the amount $\Delta\sigma$.

The maximum retention function versus temperature is determined by the temperature dependencies of the electrostatic constants (see supporting information) and of water viscosity, which affect the drag force on attached particles. The resultant temperature effects on the maximum retention function are shown in Figure 2. Higher temperature results in lower maximum concentration of attached particles, greater released particles $\sigma_{ai} - \sigma_{cr}(U, \gamma, T)$, and greater consequent permeability damage.

3. Laboratory Study

Laboratory flow-through testing in reservoir cores exhibited significant permeability decline during four sequential injections with decreasing ionic strength (see black circles in Figure 3). The details of coreflood setup can be found from Oliveira et al. [2014]. The stabilization periods greatly exceeded one PVI (pore volume injected), indicating particle transport having velocity much lower than the carrier water velocity. The effect is explained by the slow particle drift near pore walls and stagnant zones, resulting in slow average particle transport [Yuan and Shapiro, 2011; Bradford et al., 2012, 2014]. Therefore, the particle velocity is denoted as αU , $\alpha \ll 1$. The instant permeability response to ionic strength alteration, evidenced in Figure 3, justifies the maximum retention function (1–3) for particle detachment modeling.

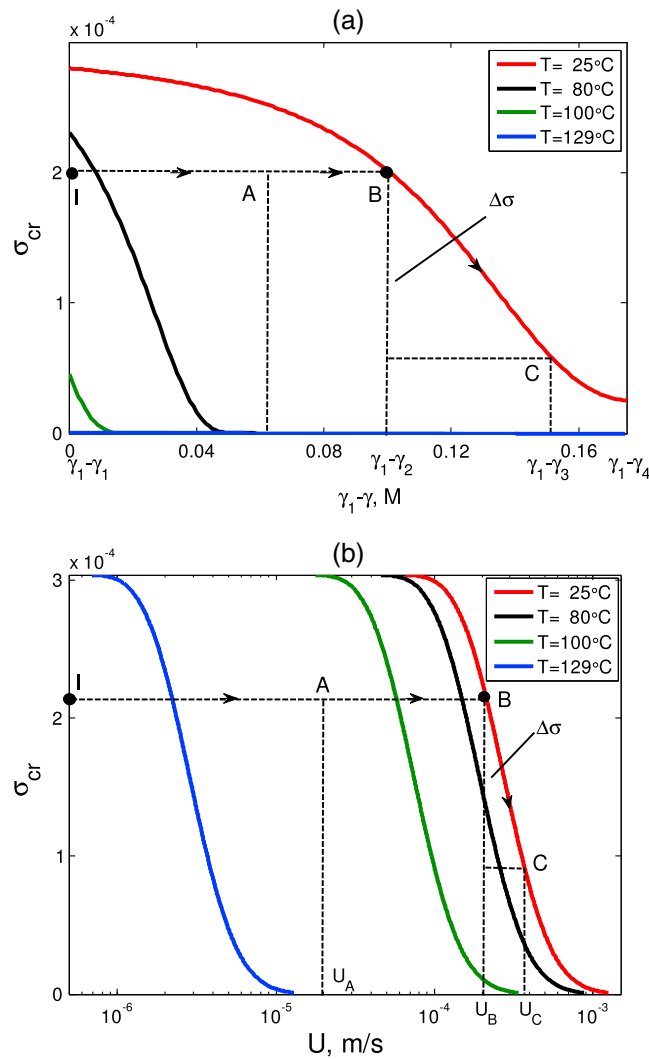


Figure 2. The maximum retention concentration σ_{cr} with (a) ionic strength (γ) dependency ($\gamma_1 = 0.2$ M NaCl) at different temperatures T and (b) velocity (U) dependency at different temperatures T .

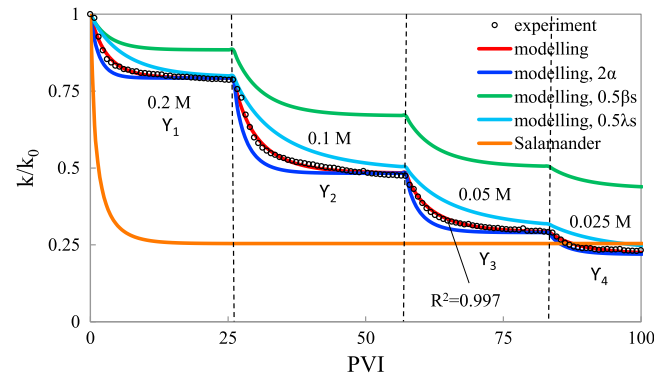


Figure 3. Tuning the laboratory data from ionic strength alteration test at $T = 25^\circ\text{C}$ by the analytical model and prediction for Salamander geothermal field ($T = 129^\circ\text{C}$): normalized permeability k/k_0 decline of the core during coreflood with piecewise decreasing ionic strength $\gamma_1 \sim \gamma_4$ (α , λ_s , and β_s are drift delay factor, filtration, and formation damage coefficients, respectively).

Equations (1)–(3) allow for transformation of the maximum retention function from ionic strength dependence to velocity dependence, i.e., $\sigma_{cr}(U, \gamma_0) = \sigma_{cr}(U_0, \gamma)$. Analysis of flow toward a wellbore, where velocity changes along the radius, requires knowledge of the maximum retention function $\sigma_{cr}(U, \gamma_0)$ (γ_0 is the ionic strength of reservoir brine). However, in laboratory experiments, ionic strength can be more readily varied over a large range than flow velocity. Therefore, ionic strength alteration was applied during coreflooding tests in the present work. The maximum retention function in Figure 2b shows the result of transformation from ionic strength dependence $\sigma_{cr}(U_0, \gamma)$ to velocity dependence $\sigma_{cr}(U, \gamma_0)$. Scanning electron microscope (SEM)-energy dispersive X-ray analysis (EDAX) results of clay particles displaced from Salamander rock fragments show illite/chlorite flakes and kaolinite platelets (Figure 4). Zeta potentials were measured for sandstone matrix and clay matter, which were recovered from the effluent during coreflooding tests. Measured values of zeta potentials were used in equations (S1)–(S4) in the supporting information for evaluation of electrostatic Derjaguin-Landau-Verwey-Overbeek (DLVO) force $F_e(U, \gamma)$, in order to calculate the maximum retention function (equations (1)–(3)).

We now compare the measured particle and pore sizes to those from modeled results. SEM images of Salamander cores show that the sizes of initially attached particles vary from 0.15 to 2.0 μm . The size range covers the variation of particle radius obtained from the maximum retention function (Figure S1 in the supporting information). Initial permeability of the fragments was $k = 6.9$ mD, and initial porosity was $\phi = 0.106$. The average pore throat size $\langle r_p \rangle$ calculated from the formula proposed by Nelson [2009] for sandstones was $\langle r_p \rangle = \sqrt{k/(4.48\phi^2)} = 5.88 \mu\text{m}$. The weighted mean radius of the breakthrough particles measured by

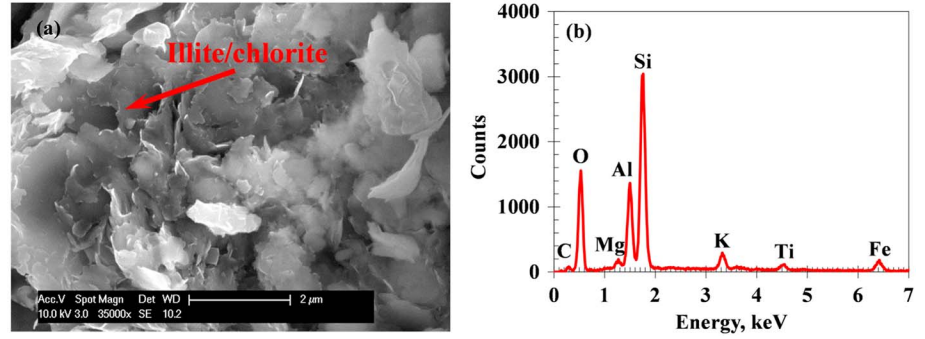


Figure 4. (a) SEM image and (b) EDAX spectrum for mixed-layer illite/chlorite clay minerals identified in the collected fines.

particle counter was $\langle r_s \rangle = 1.12 \mu\text{m}$. Particle sizes varied from 0.10 to 1.25 μm . The mean attached particle radius from modeling was $\langle r_p \rangle = 1.80 \mu\text{m}$. The filtration theory suggests that particles with radii above $\langle r_p \rangle / 3$ are captured in rocks and do not appear in the effluent [van Oort *et al.*, 1993]. Indeed, the size range of effluent particles (0.10, 1.25) was below the minimum radius of the strained particles $\langle r_p \rangle / 3 = 1.96 \mu\text{m}$, which is consistent with the filtration theory.

4. System of Governing Equations

The mathematical model for fine particle migration employed the following major assumptions: velocity of fine particle migration differs from the carrier water velocity, homogeneous reservoir, low compressibility of water, no diffusion of salt and particles, instantaneous release of attached particles according to the maximum retention function $\sigma_{cr}(U, \gamma)$, linear kinetics of particle straining by porous media, and permeability increase due to particle detachment was negligible in comparison with permeability decrease due to particle straining. In order to describe the processes of particle detachment, migration, retention in rocks, and consequent permeability reduction, the system of governing equations for fluid flow and particle transport in porous media is derived. It consists of mass balance equations for water, salt, and particles; a linear kinetics expression for capture rate; equation of state for water; and Darcy's law to account for permeability damage due to particle straining:

$$\frac{\partial}{\partial t} [(\phi - \sigma_a - \sigma_s)(1 - c)\rho_w] + \nabla \cdot [(1 - c)\rho_w \mathbf{U}] = 0 \quad (4)$$

$$\frac{\partial}{\partial t} [(\phi - \sigma_a - \sigma_s)(1 - c)\gamma\rho_w] + \nabla \cdot [(1 - c)\gamma\rho_w \mathbf{U}] = 0 \quad (5)$$

$$\frac{\partial}{\partial t} [(\phi - \sigma_a - \sigma_s)c + \sigma_a + \sigma_s] + \nabla \cdot (c\alpha \mathbf{U}) = 0 \quad (6)$$

$$\frac{\partial \sigma_s}{\partial t} = \lambda_s c \alpha |\mathbf{U}|, \rho_w = \rho_{w0} e^{c_w(p - p_0)}, \mathbf{U} = -\frac{k_0}{\mu(1 + \beta_s \sigma_s)} \nabla p \quad (7)$$

where ϕ is the porosity; c , σ_a , and σ_s are suspended, attached, and strained concentrations, respectively; ρ_w is the water density; \mathbf{U} is the velocity; p is the pressure; α is the drift delay factor; λ_s and β_s are filtration and formation damage coefficients for straining, respectively; c_w and μ are water compressibility and viscosity, respectively; and k_0 is the initial permeability [Bedrikovetsky, 1993]. In the following sections, the system of governing equations will be applied to the linear flow through core samples in laboratory tests and radial flow toward wellbore in field applications.

The maximum retention function $\sigma_a = \sigma_{cr}(U, \gamma)$ is a phenomenological relationship in the model. The particular form in equations (1)–(3) assumes simplified pore geometry and homogeneity. The stochastic models should be applied to describe geometric and chemical matrix heterogeneity [Bradford *et al.*, 2013]. For example, probability distribution of the constants in equation (1) followed by the averaging allows determination of the maximum retention function in microheterogeneous rocks.

5. History Matching of the Laboratory Flow-Through Test Results

For one-dimensional flow, under the assumptions of incompressible fluid and small concentrations c and σ_s , the coreflood problem in equations (3)–(7) with altering ionic strength allows for analytical solution similar to that presented by *Bedrikovetsky et al.* [2012]. The initial condition for suspended concentration corresponds to the release of $\Delta\sigma$ particles due to ionic strength alteration (Figure 2). Inlet boundary conditions include injected ionic strength and zero concentration of suspended particles. Least squares optimization using the analytical model yielded the following values of tuning parameters: drift factor $\alpha=0.003$, filtration coefficient $\lambda_s=53\text{ m}^{-1}$, formation damage coefficient $\beta_s=7600$, mean radius of attached particles $1.80\text{ }\mu\text{m}$, and variance coefficient for particle size distribution $C_v=0.66$. The values of permeability damage coefficients λ_s and β_s are within the common range [*Khilar and Fogler, 1998*]. Comparison between experimental and modeling data showed strong agreement ($R^2=0.997$). Size distribution of the attached particles is shown as the red curve in Figure S1.

Figure 3 presents the sensitivity study with respect to the drift factor and both filtration and formation damage coefficients. Acceleration of particles yielded faster permeability stabilization. Decrease of filtration and formation damage coefficients yielded lower formation damage.

Particle size distributions in Figure S1 correspond to 10% variation of the measured data. Fewer attached particles results in less formation damage.

The maximum attached concentration curves at different reservoir temperatures are shown in Figure 2. The constants for calculation of the maximum retention function in equations (1)–(3) are taken from the coreflood data matching (Figure 3) and correspond to the conditions of the Salamander field. Higher temperature is associated with weaker electrostatic force, lower attaching torque (1), lower maximum retention concentration, and greater amount of mobilized particles $\sigma_{ai}-\sigma_a(U)$. Therefore, well impairment increases as the reservoir temperature increases. This makes well impairment due to fine particle migration more probable in geothermal reservoirs than in conventional aquifers or oilfields.

6. Analytical Model for Flow Toward Wellbore

We now discuss axisymmetric flow toward the wellbore. Initial conditions correspond to the total of initial suspended particles in the reservoir c_0 and the amount of particles released by the drag force, with the flow velocity $q/2\pi r$:

$$t = 0 : \sigma_a = \sigma_{ai}, \sigma_s = 0, c = c_i(r) = c_0 + \frac{1}{\phi} \left[\sigma_{ai} - \sigma_{cr} \left(\frac{q}{2\pi r} \right) \right] \quad (8)$$

The initial particle straining is accounted for in the initial permeability k_0 . The boundary condition of impermeability is set on the reservoir boundary $r=r_e$; either the wellbore pressure p_w or the rate q is set at the wellbore $r=r_w$ [*Bedrikovetsky, 1993*]. Ionic strength is constant; thus, equation (5) becomes trivial.

Particles were mobilized at high velocities $U > U_i$ (see point B in Figure 2) inside the zone $r < q/2\pi U_i$, $\sigma_{ai} = \sigma_{cr}(U_i, \gamma)$, where U_i is the critical flow velocity below which particles kept immobilized. Water was assumed to be incompressible inside the mobilization zone. There was no particle migration for $r > r_i$ and the inflow of compressible fluid can be characterized by a linear parabolic pressure diffusivity equation. The exact solution of the problem in equations (3), (4), and (6) in the mobilization zone is obtained by the method of characteristics:

$$c(r, t) = c_i(r) e^{\lambda_s(r - \sqrt{r^2 + 2Bt})}, \quad B = \frac{q}{2\pi\alpha\phi} \quad (9)$$

$$\sigma_s(r, t) = \frac{\phi}{r} c_i(r) \left[r + \lambda_s^{-1} - e^{\lambda_s(r - \sqrt{r^2 + 2Bt})} \left(\sqrt{r^2 + 2Bt} + \lambda_s^{-1} \right) \right] \quad (10)$$

Pressure distribution in the mobilization zone $r_w < r < r_i$ is determined by integrating equation (7) with respect to r . Pressure distribution outside the mobilization zone $r_i < r < r_e$ is obtained by Fourier series

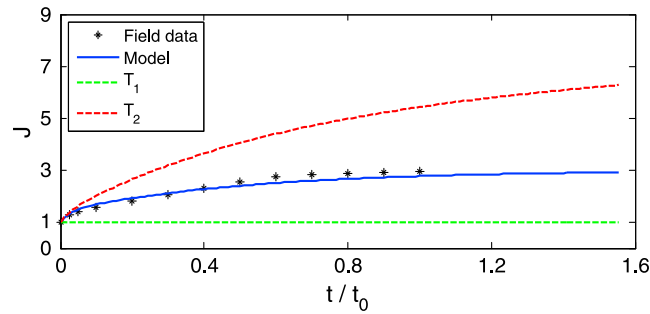


Figure 5. Well impedance J growth during well exploitation from the modeled results and field data (reservoir temperature 129°C, two other temperatures for sensitivity study: $T_1 = 25^\circ\text{C}$, $T_2 = 160^\circ\text{C}$, t/t_0 : dimensionless time).

scheme for unknowns p , ρ_w , σ_s , and σ_a [Iserles, 2009]. For conditions of the Salamander field, the difference in wellbore pressure and impedance prediction by analytical and numerical models is 2.5%.

7. Treatment of Field Data

The Salamander geothermal well was discharging for 5 h (denoted as t_0). The rate was held constant at 15.5 L/s during the production period. Pressure drawdown increased from 20 bars at the beginning of discharge to 55 bars at the end. Star points in Figure 5 correspond to the well data.

Electrostatic DLVO constants were taken to be the same as in laboratory study (section 3). Reservoir temperature $T = 129^\circ\text{C}$, permeability $k_0 = 6.9$ mD, and porosity $\phi = 0.1$. Dynamic viscosity data for NaCl solutions in water was adopted from Al-Shemmeri [2012]. The tuning parameters included filtration coefficient λ_s , formation damage coefficient β_s , and drift delay factor α . The adjustment of the analytical model in equations (9)–(11) to field data was performed using the Levenberg-Marquardt optimization algorithm to minimize the least squares deviation. The optimal values of the tuning parameters were found to be $\lambda_s = 10 \text{ m}^{-1}$, $\beta_s = 9900$, and $\alpha = 0.1$. Comparison of field data against modeling results yielded the coefficient of determination $R^2 = 0.99$ (Figure 5). The optimal parameter values fall within the intervals commonly encountered in field applications [Khilar and Fogler, 1998].

The orange curve in Figure 3 was calculated using the above Salamander field parameters and exhibits much greater formation damage than in the coreflooding test.

The sensitivity of well impedance to reservoir temperature is shown in Figure 5 for $T_1 = 25^\circ\text{C}$ and $T_2 = 160^\circ\text{C}$. The corresponding maximum retention curves are shown in Figure 2. Higher temperature was associated with lower maximum retention concentration and greater release of particles due to water inflow. However, water viscosity decreased with temperature, resulting in the decrease of the detaching drag force. The analytical model of equations (9)–(11) with the parameters tuned from the Salamander well history was used to predict impedance. Higher temperature was associated with greater formation damage; i.e., the effect of temperature on electrostatic force was much greater than that of brine viscosity. As a result, geothermal reservoirs are more susceptible to fines migration-induced productivity decline than are conventional oilfields and aquifers.

In high-permeability reservoirs with small particles, where straining does not occur, fine particle migration may not impair productivity. The above methodology of laboratory-based well-behavior prediction using the tuned mathematical model has been applied to well-productivity prediction in the geothermal field known as Celsius (Cooper/Eromanga Basin, Australia). Laboratory coreflooding tests revealed some permeability increase during fine particle migration, leading to well-productivity increase during exploitation.

8. Conclusions

Analysis of temperature dependency of fine particle migration using the experiment-based mathematical modeling supports the following conclusions:

[Polyanin, 2007]. The analytical solution allows calculating the so-called well impedance J , which is the dimensional pressure difference between the reservoir and the wellbore (Δp) per unit of the production rate (q):

$$J(t) = \Delta p(t)q(t=0) / \Delta p(t=0)q(t) \tag{11}$$

The finite difference approximations for equations (3)–(7) are solved by iterative algorithm using an implicit scheme for unknowns c and U , and an explicit

1. For geothermal reservoir conditions, the lifting and gravity forces are 2–4 orders of magnitude weaker than the drag and electrostatic forces. Mechanical equilibrium of attached particles and the maximum retention function are determined by drag and electrostatic forces;
2. The fine particle-release capacity (maximum retention function) for a monolayer deposit of multisized particles can be expressed by explicit formula;
3. Size distribution of attached particles can be determined from the maximum retention function;
4. Experiment-based model predictions for high-temperature geothermal conditions showed that the electrostatic attraction weakens with temperature increase, and the detaching drag force reduces with water viscosity decrease. The former effect dominates, resulting in the decrease of the maximum retention function with temperature. Therefore, geothermal reservoirs are more susceptible to fine particle migration than conventional aquifers or oilfields;
5. The laboratory “velocity-ionic strength” translation procedure along with the mechanical equilibrium modeling allows determining velocity dependency of the maximum retention concentration from the tests with varying ionic strength;
6. The permeability stabilization time during fine particle migration highly exceeds one pore volume injected, suggesting that the fine particle migration velocity is significantly lower than the carrier water velocity;
7. The analytical model for axisymmetric flows with fine particle mobilization, migration, and straining yields the explicit formulas for suspended and strained concentrations and for well impedance;
8. Laboratory-measured permeability history is consistent with the model prediction;
9. The prediction from laboratory-based mathematical modeling closely approximates well index history from field data.

Acknowledgments

Financial supports from the Australian Research Council (ARC) Discovery Project 1094299, ARC Linkage Projects 100100613 and 110200799, the Australian Renewable Energy Agency (ARENA), and the South Australian Centre for Geothermal Energy Research (SACGER) are gratefully acknowledged. Authors thank U. Schacht, T. Carageorgos, C. Matthews, and A. Musson (University of Adelaide) for fruitful cooperation and friendly support; Y. Yang for torque balance calculations; V. Zlotnik (University of Nebraska, USA) and O. Batelaan (Flinders University) for the critical comments and improvement of the text; and D. Levin for the editorial work to elevate the paper. Information of data is provided in the figures produced in the paper.

The Editor thanks two anonymous reviewers for their assistance in evaluating this paper.

References

- Al-Shemmeri, T. (2012), *Engineering Fluid Mechanics*, pp. 17–18, Ventus Publishing ApS, London.
- Altmann, J., and S. Ripperger (1997), Particle deposition and layer formation at the crossflow microfiltration, *J. Membr. Sci.*, *124*, 119–128.
- Bartels, J., M. Kühn, W. Schneider, C. Clauser, H. Pape, V. Meyn, and I. Lajcsak (2002), Core flooding laboratory experiment validates numerical simulation of induced permeability change in reservoir sandstone, *Geophys. Res. Lett.*, *29*(9), 1320, doi:10.1029/2002GL014901.
- Bedrikovetsky, P. (1993), *Mathematical Theory of Oil and Gas Recovery*, Kluwer Acad., London.
- Bedrikovetsky, P., F. D. Siqueira, C. A. Furtado, and A. L. S. Souza (2011), Modified particle detachment model for colloidal transport in porous media, *Transp. Porous Media*, *86*, 353–383.
- Bedrikovetsky, P., A. Zeinijahromi, F. D. Siqueira, C. A. Furtado, and A. L. S. de Souza (2012), Particle detachment under velocity alternation during suspension transport in porous media, *Transp. Porous Media*, *91*, 173–197.
- Boutt, D. F., G. Grasselli, J. T. Fredrich, B. K. Cook, and J. R. Williams (2006), Trapping zones: The effect of fracture roughness on the directional anisotropy of fluid flow and colloid transport in a single fracture, *Geophys. Res. Lett.*, *33*, L21402, doi:10.1029/2006GL027275.
- Bradford, S. A., S. Torkzaban, H. Kim, and J. Simunek (2012), Modeling colloid and microorganism transport and release with transients in solution ionic strength, *Water Resour. Res.*, *48*, W09509, doi:10.1029/2012WR012468.
- Bradford, S. A., S. Torkzaban, and A. Shapiro (2013), A theoretical analysis of colloid attachment and straining in chemically heterogeneous porous media, *Langmuir*, *29*, 6944–6952.
- Bradford, S. A., Y. Wang, H. Kim, S. Torkzaban, and J. Šimůnek (2014), Modeling microorganism transport and survival in the subsurface, *J. Environ. Qual.*, *43*, 421–440.
- Chen, C., A. I. Packman, and J.-F. Gaillard (2008), Pore-scale analysis of permeability reduction resulting from colloid deposition, *Geophys. Res. Lett.*, *35*, L07404, doi:10.1029/2007GL033077.
- Edey, Y., A. Kostinski, and B. Berkowitz (2011), Record setting during dispersive transport in porous media, *Geophys. Res. Lett.*, *38*, L16403, doi:10.1029/2011GL048558.
- Elimelech, M., X. Jia, J. Gregory, and R. Williams (1998), *Particle Deposition and Aggregation: Measurement, Modelling and Simulation*, Butterworth-Heinemann, Oxford.
- Freitas, A. M., and M. M. Sharma (2001), Detachment of particles from surfaces: An AFM study, *J. Colloid Interface Sci.*, *233*, 73–82.
- Gaillard, J.-F., C. Chen, S. H. Stonedahl, B. L. T. Lau, D. T. Keane, and A. I. Packman (2007), Imaging of colloidal deposits in granular porous media by X-ray difference micro-tomography, *Geophys. Res. Lett.*, *34*, L18404, doi:10.1029/2007GL030514.
- Iserles, A. (2009), *A First Course in the Numerical Analysis of Differential Equations*, Cambridge Univ. Press, Cambridge, U. K.
- Israelachvili, J. N. (2011), *Intermolecular and Surface Forces*, 3rd ed., Elsevier, Amsterdam.
- Kalantariasl, A., and P. Bedrikovetsky (2014), Stabilization of external filter cake by colloidal forces in “well-reservoir” system, *Ind. Eng. Chem. Res.*, *53*, 930–944.
- Khilar, K., and S. Fogler (1998), *Migration of Fines in Porous Media*, Kluwer Acad., Dordrecht, Netherlands.
- Kim, M., and A. L. Zydny (2004), Effect of electrostatic, hydrodynamic, and Brownian forces on particle trajectories and sieving in normal flow filtration, *J. Colloid Interface Sci.*, *269*, 425–431.
- Liu, W., and M. Manga (2009), Changes in permeability caused by dynamic stresses in fractured sandstone, *Geophys. Res. Lett.*, *36*, L20307, doi:10.1029/2009GL039852.
- Manga, M., I. Beresnev, E. E. Brodsky, J. E. Elkhoury, D. Elsworth, S. E. Ingebritsen, D. C. Mays, and C.-Y. Wang (2012), Changes in permeability caused by transient stresses: Field observations, experiments, and mechanisms, *Rev. Geophys.*, *50*, RG2004, doi:10.1029/2011RG000382.
- Mangane, P. O., P. Gouze, and L. Luquot (2013), Permeability impairment of a limestone reservoir triggered by heterogeneous dissolution and particles migration during CO₂-rich injection, *Geophys. Res. Lett.*, *40*, 4614–4619, doi:10.1002/grl.50595.

- Nelson, P. H. (2009), Pore-throat sizes in sandstones, tight sandstones, and shales, *AAPG Bull.*, 93, 329–340.
- Nemati, M. R., O. Banton, J. Caron, and L. Delaporte (2003), Contamination by slaked fragments with sorbed compounds in a structured soil, *Soil Sci. Soc. Am. J.*, 67, 694–702.
- Ochi, J., and J.-F. Vernoux (1998), Permeability decrease in sandstone reservoirs by fluid injection hydrodynamic and chemical effects, *J. Hydrol.*, 208, 237–248.
- Oliveira, M., A. Vaz, F. Siqueira, Y. Yang, Z. You, and P. Bedrikovetsky (2014), Slow migration of mobilised fines during flow in reservoir rocks: Laboratory study, *J. Petrol. Sci. Eng.*, 122, 534–541.
- Polyanin, A. D. (2007), *Handbook of Mathematics for Engineers and Scientists*, Chapman and Hall/CRC, Boca Raton, Fla.
- Rehg, K. J., A. I. Packman, and J. Ren (2005), Effects of suspended sediment characteristics and bed sediment transport on streambed clogging, *Hydrol. Processes*, 19, 413–427.
- Rosenbrand, E., C. Haugwitz, P. S. M. Jacobsen, C. Kjølter, and I. L. Fabricius (2014), The effect of hot water injection on sandstone permeability, *Geothermics*, 50, 155–166.
- Rosenbrand, E., C. Kjølter, J. F. Riis, F. Kets, and I. L. Fabricius (2015), Different effects of temperature and salinity on permeability reduction by fines migration in Berea sandstone, *Geothermics*, 53, 225–235.
- Saiers, J. E., and J. N. Ryan (2005), Colloid deposition on non-ideal porous media: The influences of collector shape and roughness on the single-collector efficiency, *Geophys. Res. Lett.*, 32, L21406, doi:10.1029/2005GL024343.
- Sefrioui, N., A. Ahmadi, A. Omari, and H. Bertin (2013), Numerical simulation of retention and release of colloids in porous media at the pore scale, *Colloids Surf. A*, 427, 33–40.
- van Oort, E., J. F. G. van Velzen, and K. Leerlooijer (1993), Impairment by suspended solids invasion: Testing and prediction, *SPE Prod. Facil.*, 8, 178–183.
- You, Z., Y. Osipov, P. Bedrikovetsky, and L. Kuzmina (2014), Asymptotic model for deep bed filtration, *Chem. Eng. J.*, 258, 374–385.
- Yuan, H., and A. A. Shapiro (2011), Induced migration of fines during waterflooding in communicating layer-cake reservoirs, *J. Petrol. Sci. Eng.*, 78, 618–626.